PERGAMON

International Journal of Heat and Mass Transfer 44 (2001) 1837–1848

International Journal of HEAT and MASS TRANSFER

www.elsevier.com/locate/ijhmt

A new numerical formulation for incompressible viscous free surface flow without smearing the free surface

S.L. Lee *, S.R. Sheu

Department of Power Mechanical Engineering, National Tsing-Hua University, Hsinchu 30043, Taiwan, ROC

Received 18 November 1999; received in revised form 26 July 2000

Abstract

A new numerical formulation is presented in this paper for incompressible viscous free surface flow without smearing the free surface. Laws of conservation for the entire physical domain, including both liquid and air, are formulated with a single set of governing equations. To properly handle the discontinuities of the physical properties across the free surface, an extended weighting function scheme is developed for the numerical solution on a fixed and nonstaggered Cartesian grid system. Unlike existing numerical methods, the force balance equation is imposed on the free surface through the use of the NAPPLE algorithm without smearing the free surface. During the solution procedure, a harmonic function referred as an "extrapolated velocity" from the liquid is computed based on the velocity solution at the grid points adjacent to the free surface on the liquid side. With a migration velocity interpolated from such a harmonic function, the free surface profile for the next time step is estimated. This gives rise to a smooth free surface profile and thus circumvents high frequency noises on the curvature of the resulting free surface. Furthermore, advancement of the free surface is not restricted to one grid mesh in a single time step. Performance of the present method is examined through three well-documented dam-breaking examples. The results reveal the existence of an induced vortex in a layer of air adjacent to the free surface. Good agreement between the computed water front and the experimental data is observed. Although only two-dimensional cases are demonstrated in this paper, concept of the present numerical method is equally applicable to three-dimensional problems with moving free surfaces. It also applies to convective heat and mass transfer problems such as filling process in gravity and die casting processing.

1. Introduction

Incompressible viscous flow with a moving free surface has many applications in industry and in nature such as environment engineering, die casting, injection molding process, and many others. The available numerical methods for such problems can be classified into moving and fixed grid approaches. Moving grid approach is typically confined to special applications due to limitations in the rezoning technique [1–3]. In this connection, the fixed grid approach seems to be a more viable method whenever a general motion of free surface flow (e.g., the filling process in die casting [4]) is solved.

Among the existing fixed grid approaches, Harlow and Welch [5] proposed the well-known maker and cell method (MAC) that labels fluid particles with markers. Recently, Nakayama and Mori [6] improved the MAC method to preclude the possibility of producing an unphysical liquid front advancement. In the use of the MAC method, the region occupied by the fluid is tracked by the locations of the markers in the course of fluid motion. Such a method defines the fluid region rather than the free surface, and thus requires large computer storage and additional computational time to move all the fluid markers to new locations especially when a three-dimensional problem is encountered [7]. Furthermore, a finite volume far from the free surface might be unrealistically overfilled or partially filled with markers due to numerical errors. To circumvent the disadvantages of the MAC method, Raad et al. [8]

* Corresponding author. Fax: +886-3-572-8230.
E-mail address: sllee@pme.nthu.edu.tw (S.L. Lee).

0017-9310/01/$ - see front matter
PII: S0017-9310(00)00247-7

Nomenclature

f	volume fraction of liquid
g	gravity, 9.806 ms^{-2}
H	original height of water column [m]
$h(x)$	dimensionless free surface profile
P, P_∞	pressure and referenced pressure [N m^{-2}]
p	dimensionless pressure, $(P-P_\infty)/(\rho_l U_c^2)$
Re	Reynolds number, $\rho_l U_c H/\mu_l$
t	time [s]
(U, V)	velocity [ms^{-1}]
U_c	characteristic velocity, $\sqrt{gH}$
(u, v)	dimensionless velocity, $(U/U_c, V/U_c)$
W	original width of water column [m]
We	Weber number, $\rho_l U_c^2 H/\gamma$
$w_f(z)$	weighting function, $z/(1-\exp(-z))$
$\hat{w}_f$	extended weighting function (18)
(X, Y)	coordinates [m]
(x, y)	dimensionless coordinates, $(X/H, Y/H)$
x_f	water front
z	grid Peclet number (15)

Greek symbols

γ	coefficient of surface tension [N m^{-1}]
$\Delta x_i, \Delta y_j$	grid meshes
$\Delta\tau$	time step
κ	curvature of the free surface [m^{-1}]
μ	viscosity [N s m^{-2}]
μ^*	dimensionless viscosity, μ/μ_l
ρ	density [kg m^{-3}]
ρ^*	dimensionless density, ρ/ρ_l
σ_{nn}	normal stress on the free surface (19b)
τ	dimensionless time, $(U_c/H)t$
τ_0	previous time, $\tau-\Delta\tau$

Subscripts

0	quantity at time τ_0
a	air
l	liquid
w	water

suggested the use of micro cells and markers only in a region near the free surface. In their micro cell method (MIC), the movement of the free surface was accomplished by tracking the massless markers on the free surface.

In 1981, Hirt and Nichols [9] introduced the volume of fluid method (VOF) for incompressible flow with a moving free surface. The VOF method is based on the concept of a fractional volume of liquid inside a finite volume [10]. A finite volume fully filled with liquid is denoted by $f=1$, while an empty finite volume has the value of $f=0$. For a finite volume containing the free surface, the fractional volume of liquid would be $0<f<1$. Hirt and Nichols [9] claimed that location of the free surface can be determined from f and its normal direction, although f is a step function across the free surface. However, there are a few disadvantages in the use of the VOF method as remarked by Wang and Wang [11]. First, a partially filled finite volume could be surrounded by non-empty finite volumes and thus be considered filled. Second, empty or partially filled finite volume could be overfilled when the free surface advances. Third, the computational domain would suddenly change whenever a non-empty finite volume becomes filled or surrounded by other non-empty finite volume. This sudden change could cause numerical instability and/or unphysical results for the velocity and pressure near the free surface.

One of the major difficulties in solving a moving free surface problem is the prediction of the free surface advancement. In the VOF method, location of the free surface is estimated by using a donor–acceptor algorithm. However, implementation of donation and reception of liquid is restricted to only between adjacent finite volumes. Material moving through more than one finite volume is not allowed in a single time step. As a result, the time step would be very small, especially when a fine grid system is desired. Furthermore, the numerical procedure becomes very cumbersome when the VOF method is applied to three-dimensional problems. In three-dimensional cases, 64 and 24 different arrangements must be checked, respectively, for the satisfaction of mass conservation and no-shear condition on the free surface [4].

In their net inflow method, Wang and Wang [11] proposed a finite element procedure to simulate incompressible viscous flow with a moving free surface. A layer of air near the free surface was considered with the motion of liquid in a fixed grid system. An artificial viscosity is then employed to force the velocity of the air to follow the liquid velocity on the free surface. Finally, the liquid in each finite volume is calculated by directly integrating the net inflow rate of liquid with respect to time. However, the free surface in the net inflow method cannot advance over more than one grid mesh in a single time step as in most existing methods. In addition, the liquid front based on the net inflow method was found to have a contact angle of about 90° on the wall. This does not seem to be consistent with the experimental observation [12].

Recently, Wu et al. [13] applied the continuum surface force method (CSF) on the dam-breaking problem. The CSF method was introduced by Brackbill et al. [14] and improved later by Jacqmin [15]. In this particular numerical method, a color function similar to f in the VOF method is smeared in a layer of finite thickness instead of the original sharp step function. All the

physical properties such as the density and the viscosity are then assumed to be linear functions of the color function that vary smoothly across the artificial thickness of a smeared free surface. Similar concept (smearing the free surface) seems to play the leading role in the recent development of numerical methods for free surface flow such as the indicator function [16] and the level set function [17]. Unfortunately, very fine grids are generally needed in the use of a smearing function (e.g., VOF, color function, indicator function and level set function) due to the irregular shape of the moving free surface. Otherwise, gradients of the smeared physical quantities as well as the migration velocity of the free surface cannot be properly handled as pointed out by Haj-hariri et al. [18].

The purpose of the present study is to propose a new numerical formulation for incompressible viscous free surface flow without smearing the free surface. The sharp jumps of the physical properties across the free surface will be handled by an extended weighting function scheme. A particular harmonic function is then introduced to estimate the migration velocity of the free surface. Through the use of the NAPPLE algorithm, a force balance equation including surface tension is imposed on the free surface. Performances of the proposed numerical procedure will be examined through three well-documented dam-breaking examples.

2. Governing equations

Consider a two-dimensional liquid column of height H and width W at the corner $0 \leqslant X \leqslant W$, $0 \leqslant Y \leqslant H$. The liquid column, initially at rest, collapses onto the horizontal dry plane ($Y = 0$, $X \geqslant 0$) at $t > 0$. The liquid spreads out and the height of the column falls. The flow is laminar and incompressible. All the physical properties are assumed to be constant for simplicity. After introducing the dimensionless transformation

$$\begin{aligned} &x = X/H, \quad y = Y/H, \quad u = U/U_c, \\ &v = V/U_c, \quad p = (P - P_\infty)/(\rho_l U_c^2), \\ &\tau = (U_c/H)t, \quad Re = \rho_l U_c H/\mu_l, \quad U_c = \sqrt{gH}, \\ &\rho^* = \rho/\rho_l, \quad \mu^* = \mu/\mu_l \end{aligned} \tag{1}$$

a single set of governing equations covering both the liquid and the surrounding air can be written as

$$\frac{\partial u}{\partial x} + \frac{\partial v}{\partial y} = 0, \tag{2}$$

$$\rho^*\left(\frac{\partial u}{\partial \tau} + u\frac{\partial u}{\partial x} + v\frac{\partial u}{\partial y}\right) = -\frac{\partial p}{\partial x} + \frac{1}{Re}\left(\frac{\partial}{\partial x}\left(\mu^*\frac{\partial u}{\partial x}\right) + \frac{\partial}{\partial y}\left(\mu^*\frac{\partial u}{\partial y}\right)\right), \tag{3}$$

$$\rho^*\left(\frac{\partial v}{\partial \tau} + u\frac{\partial v}{\partial x} + v\frac{\partial v}{\partial y}\right) = -\frac{\partial p}{\partial y} - \rho^* + \frac{1}{Re}\left(\frac{\partial}{\partial x}\left(\mu^*\frac{\partial v}{\partial x}\right) + \frac{\partial}{\partial y}\left(\mu^*\frac{\partial v}{\partial y}\right)\right). \tag{4}$$

Mathematically, the dimensionless density ρ^* and viscosity μ^* are step functions across the free surface. They have the value of unity in the liquid region and jump to another constant in the air region, i.e.

$$\rho^* = \begin{cases} 1 & \text{in liquid,} \\ \rho_a/\rho_l & \text{in air,} \end{cases} \tag{5}$$

$$\mu^* = \begin{cases} 1 & \text{in liquid,} \\ \mu_a/\mu_l & \text{in air,} \end{cases} \tag{6}$$

where the subscripts a and l denote the properties of the air and the liquid, respectively.

Conventionally, the free-slip condition is imposed on all the solid boundaries $x = 0$ and $y = 0$ for free surface problem [3,5,6,13]. This does not seem to be consistent with the theory of viscous flow. By contrast, the use of the no-slip condition gives rise to a particular numerical difficulty that the liquid front on the solid wall would never advance. Due to the lack of a reliable dynamic model for the contact angle at the liquid front, the partial-slip condition

$$\xi\frac{\partial u}{\partial y} + (1 - \xi)u = 0, \quad v = 0, \tag{7a}$$

$$\xi = \begin{cases} \dfrac{x - x_a}{x_f - x_a} & \text{for } x_a \leqslant x \leqslant x_f, \\ \dfrac{x - x_b}{x_f - x_b} & \text{for } x_f \leqslant x \leqslant x_b, \\ 0 & \text{otherwise} \end{cases} \tag{7b}$$

on the horizontal plane $y = 0$ is employed in a local area $x_a \leqslant x \leqslant x_b$ covering the liquid front x_f. Receding of the liquid column on the vertical wall $x = 0$ is treated similarly. The artificial boundary condition (7a) and (7b) would be a good approximation as long as the characteristic length of the problem is sufficiently large.

3. The extended weighting function scheme

Eqs. (2)–(4) and the appropriate boundary condition (7a) and (7b) constitute a system of partial differential equations. In the present study, the solution procedure is performed on a regular (nonstaggered) Cartesian grid system (x_i, y_j) with the simple notations

$$\Delta x_i = x_{i+1} - x_i, \quad \overline{\Delta x}_i = (\Delta x_{i-1} + \Delta x_i)/2, \tag{8a}$$

$$\Delta y_j = y_{j+1} - y_j, \quad \overline{\Delta y}_j = (\Delta y_{j-1} + \Delta y_j)/2. \tag{8b}$$

For convenience, let the finite area $\overline{\Delta x}_i \times \overline{\Delta y}_j$ containing the grid point $P(x_i, y_j)$ be referred as "finite volume of point P". The four points adjacent to point P are denoted, respectively, by $W(x_{i-1}, y_j)$, $E(x_{i+1}, y_j)$, $S(x_i, y_{j-1})$, $N(x_i, y_{j+1})$. Due to the finite size of the grid mesh, a finite volume on the free surface would cover both regions of liquid and air. Under such a situation, the density ρ^* appearing in the unsteady terms of Eqs. (3) and (4) and the body force term in Eq. (4) should be evaluated from

$$\rho^* = \overline{\rho}^* = f + (1-f)\rho_a/\rho_l, \tag{9}$$

where $\overline{\rho}^*$ is the dimensionless average density and f is the volume fraction of the liquid inside the finite volume. Nevertheless, simply assigning $\rho^* = 1$ and $\rho^* = \rho_a/\rho_l$ when point P is in liquid and in air respectively, would not show significant error.

Next, applying the integration scheme [19] on Eq. (4) for the grid point $P(x_i, y_j)$, one has

$$(a_W)_{i,j} v_{i-1,j} + (a_E)_{i,j} v_{i+1,j} + (a_S)_{i,j} v_{i,j-1} + (a_N)_{i,j} v_{i,j+1} - (a_P)_{i,j} v_{i,j} = (a_R)_{i,j} + Re \frac{\partial p}{\partial y}, \tag{10}$$

$$(a_W)_{i,j} = \left(\overline{\Delta x}_i \int_{x_{i-1}}^{x_i} \frac{1}{\mu^*} \exp\left(- \int_x^{x_i} \frac{Re\rho^* u}{\mu^*} \, dx \right) dx \right)^{-1}, \tag{11a}$$

$$(a_E)_{i,j} = \left(\overline{\Delta x}_i \int_{x_i}^{x_{i+1}} \frac{1}{\mu^*} \exp\left(\int_{x_i}^{x} \frac{Re\rho^* u}{\mu^*} \, dx \right) dx \right)^{-1}, \tag{11b}$$

$$(a_S)_{i,j} = \left(\overline{\Delta y}_j \int_{y_{j-1}}^{y_j} \frac{1}{\mu^*} \exp\left(- \int_y^{y_j} \frac{Re\rho^* v}{\mu^*} \, dy \right) dy \right)^{-1}, \tag{11c}$$

$$(a_N)_{i,j} = \left(\overline{\Delta y}_j \int_{y_j}^{y_{j+1}} \frac{1}{\mu^*} \exp\left(\int_{y_j}^{y} \frac{Re\rho^* v}{\mu^*} \, dy \right) dy \right)^{-1}, \tag{11d}$$

$$(a_P)_{i,j} = (a_W)_{i,j} + (a_E)_{i,j} + (a_S)_{i,j} + (a_N)_{i,j} + Re\, \overline{\rho}^*/\Delta\tau, \tag{12}$$

$$(a_R)_{i,j} = Re\overline{\rho}^*(1 - v_0/\Delta\tau), \tag{13}$$

where v_0 is the velocity at the previous time step ($\tau_0 = \tau - \Delta\tau$). If both ρ^* and μ^* are continuous in the interval $x_i \leqslant x \leqslant x_{i+1}$ on $y = y_j$, then the weighting factors $(a_E)_{i,j}$ and $(a_W)_{i+1,j}$ reduce to the standard weighting function scheme [20]

$$(a_E)_{i,j} = \frac{\mu^* w_f(-z)}{\Delta x_i \overline{\Delta x}_i}, \qquad (a_W)_{i+1,j} = \frac{\mu^* w_f(z)}{\Delta x_i \overline{\Delta x}_{i+1}}, \tag{14}$$

$$w_f(z) = \frac{z}{1 - \exp(-z)},$$

$$z = Re\, \overline{u}(\rho^*/\mu^*)\Delta x_i, \qquad \overline{u} = \frac{1}{\Delta x_i} \int_{x_i}^{x_{i+1}} u \, dx, \tag{15}$$

where the function $w_f(z)$ is known as the weighting function [20] while z is the grid Peclet number in the interval $x_i \leqslant x \leqslant x_{i+1}$.

In case the free surface intersects the interval $x_i \leqslant x \leqslant x_{i+1}$ at $x = x_s$, one should integrate Eqs. (11a)–(11d) piece by piece over the two subintervals $x_i \leqslant x \leqslant x_s$ and $x_s \leqslant x \leqslant x_{i+1}$ as demonstrated in [19, Eqs. (15a) and (16)]. Once this is done, the weighting factors in the interval $x_i \leqslant x \leqslant x_{i+1}$ are expressible as:

$$(a_E)_{i,j} = \hat{w}_f(-z_1, -z_2 \,|\, (\rho^*)_1, (\rho^*)_2, (\mu^*)_1, (\mu^*)_2)/(\Delta x_i \overline{\Delta x}_i), \tag{16a}$$

$$(a_W)_{i+1,j} = \hat{w}_f(z_2, z_1 \,|\, (\rho^*)_2, (\rho^*)_1, (\mu^*)_2, (\mu^*)_1)/(\Delta x_i \overline{\Delta x}_{i+1}), \tag{16b}$$

where

$$z_1 = Re(\overline{u})_1(\rho^*/\mu^*)_1 \Delta s_1, \tag{17a}$$

$$z_2 = Re(\overline{u})_2(\rho^*/\mu^*)_2 \Delta s_2, \tag{17b}$$

$$\hat{w}_f(\alpha, \beta \,|\, a_1, a_2, b_1, b_2) = \frac{a_2 b_1 \alpha + a_1 b_2 \beta}{a_2(1 - \exp(-\alpha)) + a_1(1 - \exp(-\beta))\exp(-\alpha)}. \tag{18}$$

In Eqs. (16a), (16b), (17a) and (17b), the subscripts 1 and 2 represent, respectively, the subintervals $x_i \leqslant x \leqslant x_s$ and $x_s \leqslant x \leqslant x_{i+1}$, while $\Delta s_1 = x_s - x_i$ and $\Delta s_2 = x_{i+1} - x_s$. Due to the no-slip condition on the free surface, letting $(\overline{u})_2/(\overline{u})_1 = 1$ would make a good approximation for the scheme, although the velocity gradient could be discontinuous across the free surface. For simplicity, the parameter $(\overline{u})_2/(\overline{u})_1$ has been removed from the $\hat{w}_f$ function (18). With this same procedure, the other weighting factors in Eqs. (11c) and (11d) can be written in a form similar to Eqs. (16a) and (16b).

It is noteworthy that the weighting factors (16a) and (16b) will become the standard weighting function scheme (14) if one assigns either $(\Delta s_1, \Delta s_2) = (\Delta x_i, 0)$ or $(\rho^*)_1 = (\rho^*)_2$, $(\mu^*)_1 = (\mu^*)_2$, $\overline{u}_1 = \overline{u}_2 = \overline{u}$, $z_1 + z_2 = z$ for an interval without free surface. Hence, the present scheme (16a) and (16b) is called "extended weighting function scheme". In the present formulation, the "free surface" turns out to be an internal boundary of the physical domain, and thus no additional treatment is needed for the shear stress on the free surface.

4. Numerical procedure

It is interesting to note that both liquid and air could be incompressible even though their densities are significantly different. Thus, the law of "volume conservation" (Eq. (2)) is valid for the entire computational domain including the free surface itself and both regions of liquid and air. This implies the applicability of the NAPPLE algorithm [21] on a nonstaggered grids covering the entire flow configuration under study. In the present computations, velocity and pressure (u, v, p) under a given free surface is solved by using the extended weighting function scheme along with the NAPPLE algorithm and the strongly implicit solver [22]. Through the use of the NAPPLE algorithm, the pressure p_l as depicted in Fig. 1 is imposed on the liquid-side of the free surface when the pressure-linked equation is solved. In this connection, effect of surface tension can be taken into account by considering the force balance equation on the free surface [23,24]

$$p_l = p_a + \frac{\kappa H}{We} + \frac{1}{Re}\left((\sigma_{nn})_l - \left(\frac{\mu_a}{\mu_l}\right)(\sigma_{nn})_a\right), \tag{19a}$$

$$We = \frac{\rho_l U_c^2 H}{\gamma} = \frac{\rho_l g H^2}{\gamma}, \qquad \sigma_{nn} = 2\frac{\partial v_n}{\partial n}, \tag{19b}$$

where γ, κ and We are the coefficient of surface tension, the curvature of a convex free surface profile, and the Weber number, respectively. The notations $(\sigma_{nn})_l$ and $(\sigma_{nn})_a$ denote, respectively, the dimensionless normal stresses on liquid-side and air-side of the free surface, while $\partial v_n/\partial n$ represents the dimensionless normal strain rate on the free surface. Determination of the air-side pressure p_a will be discussed later.

Generally speaking, after the solution (u, v, p) converges, the velocity on the free surface cannot be precisely interpolated from the velocity solution at the grid points due to the discontinuity of the velocity gradient across the free surface. To resolve this problem, a particular numerical technique is proposed. Fig. 2 shows a schematic free surface in a computational domain with a fixed and nonstaggered Cartesian grid system. The grid points (the white nodes) adjacent to the free surface on the liquid side separate the computational domain into two regions. One of the two regions contains only liquid, while the other (the gray region) includes the whole air region, the free surface and a narrow liquid layer between the white nodes and the free surface. Let the Laplace equations

$$\frac{\partial^2 u^*}{\partial x^2} + \frac{\partial^2 u^*}{\partial y^2} = 0, \qquad \frac{\partial^2 v^*}{\partial x^2} + \frac{\partial^2 v^*}{\partial y^2} = 0 \tag{20}$$

be solved in the gray region with known velocities at the white nodes. The resulting *harmonic functions* $u^*(x, y)$ and $v^*(x, y)$, for convenience, will be referred as "extrapolated velocity from the liquid region". The migration velocity of the free surface is then interpolated from the "extrapolated velocity". Undoubtedly, the extrapolated velocity could produce a smoothly varying velocity on the free surface. It is noted that the Laplace Eqs. (20) are used only to extrapolate the liquid velocity in a narrow region covering the free surface. Influence of

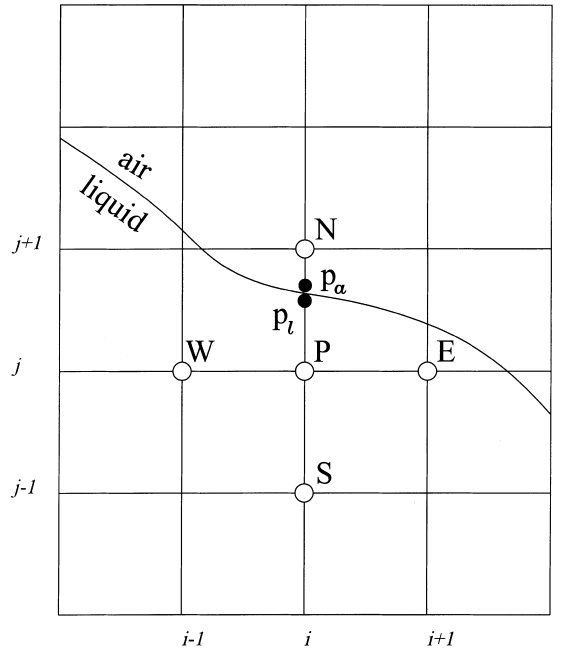

Fig. 1. Free surface pressures p_l and p_a on a fixed and nonstaggered Cartesian grid system.

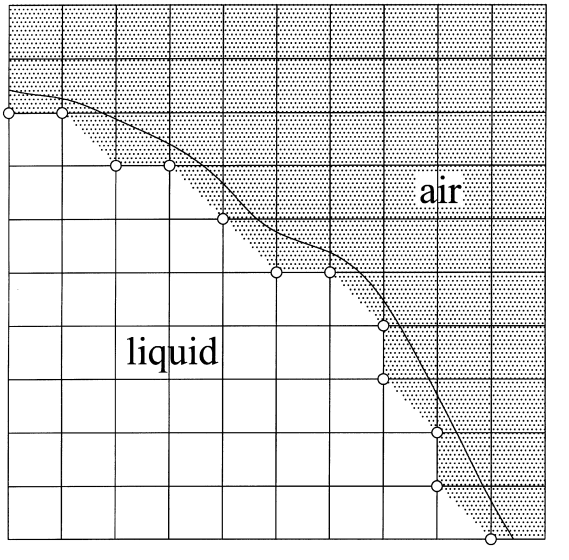

Fig. 2. The domain (gray region) where the extrapolated velocity (u^*, v^*) is defined.

other boundary conditions is not significant. Hence, when Eq. (20) is solved, zero velocity $(u^*, v^*) = (0, 0)$ is assumed on all the computational boundaries except for the white nodes (see Fig. 2), and $\partial u^*(x, 0)/\partial y = 0$ and $\partial v^*(0, y)/\partial x = 0$ for simplicity.

Once the migration velocity of the free surface is determined, the position of the free surface for the next time step can be estimated by tracing the marker strings [25] on the free surface. To achieve a good accuracy, spacing of the markers is maintained essentially in the order of $(\Delta x/10)$. However, each marker could receive an individual random error due to the explicit marker tracing. This implies the existence of high frequency numerical errors in the estimated free surface $h(x)$ that could lead to unstable surface tension results. In the present study, the filter

$$\overline{h}_k = \frac{1}{5}\sum_{m=k-2}^{k+2} h_m, \qquad \overline{x}_k = \frac{1}{5}\sum_{m=k-2}^{k+2} x_m \tag{21}$$

is used to filter out the high frequency error, where (x_m, h_m) denotes the coordinate of the mth marker before being filtered. The scale of the filter (21) is only one-half of a grid mesh $(\Delta x/2)$ and thus does not influence the resolution of the numerical solution. This same numerical technique can be implemented in three-dimensional flows if an unstructured triangle element system [16] is employed for the definition of the free surface profile.

For convenience, the present numerical procedure is summarized as follows.

1. Given the profile of the free surface $h_0(x)$ and velocity (u_0, v_0) at the previous time level τ_0.
2. Based on (u_0, v_0, h_0), solve Eq. (20) in the gray region with the known velocities at the white nodes (see Fig. 2) to yield an extrapolated velocity from the liquid region.
3. Use the extrapolated velocity to interpolate the migration velocity of the free surface.
4. Determine the position of the free surface $h(x)$ with Eq. (21) for the present time level $\tau = \tau_0 + \Delta\tau$.
5. Replace the air velocity (u_0, v_0) with the extrapolated velocity in the narrow layer where the advancing free surface sweeps through during the period from τ_0 to $\tau_0 + \Delta\tau$.
6. Based on the free surface $h(x)$ from step 4 and the modified velocity (u_0, v_0) from step 5, solve the governing equations (2)–(4) to obtain the solution (u, v, p) for the present time level τ.
7. Stop the computations if the prescribed time limit has been reached. Otherwise, set $\tau_0 = \tau$ and $(u_0, v_0, h_0) = (u, v, h)$, then return to step 2 and repeat the computations.

The solution procedure for the governing equations (2)–(4) mentioned in step 6 is expressible as the following numerical loop.

(a) Guess a solution (u, v, p) for the present time level τ.
(b) Estimate the air pressure p_a on the liquid–air interface from the guessed pressure in the air region with a procedure similar to that described in steps 2 and 3 for the interface velocity. In this connection, zero normal pressure-gradient is assumed on the boundaries $x = 0$ and $y = 0$.
(c) Evaluate p_l from Eqs. (19a) and (19b) for the interface pressure on the liquid side.
(d) Solve the momentum equations (3) and (4) with the extended weighting function scheme 10, (11a)–(11d), (12), (13) for (u, v).
(e) Solve Eq. (20) in the gray region with the known velocities at the white nodes (see Fig. 2) to yield an extrapolated velocity from the liquid region.
(f) Use the extrapolated velocity to interpolate the migration velocity of the free surface.
(g) Use the weighting function scheme [20] and the free surface velocity obtained in step (f) to filter out the velocity noises in the air region near the free surface.
(h) Use the NAPPLE algorithm to determine the pressure field for both liquid and air. In the meanwhile, the pressure p_l from step (c) and the free surface velocity from step (f) are imposed, respectively, on the liquid-side and the air-side of the free surface.
(i) Update the solution (u, v, p) with an SOR factor, and return to step (b) until the solution converges to a prescribed tolerance.

5. Results and discussion

Three cases of the dam-breaking problem are conducted in this section to examine the performance of the present numerical procedure. Water and air are adopted as the media of the flow. Their density and viscosity at 25°C are

$$\rho_w = 998\ \text{kg/m}^3, \qquad \mu_w = 0.99 \times 10^{-3}\ \text{kg/m s}, \tag{22a}$$

$$\rho_a = 1.205\ \text{kg/m}^3, \qquad \mu_a = 1.81 \times 10^{-5}\ \text{kg/m s}, \tag{22b}$$

$$\rho_a/\rho_w = 0.001207, \qquad \mu_a/\mu_w = 0.01828, \tag{22c}$$

$$\gamma = 0.0720\ \text{N/m} \tag{22d}$$

while the gravity is $g = 9.806\ \text{m/s}^2$. The dimensions of the water column (H, W) of the three cases are (2.25 in, 2.25 in), (4.50 in, 2.25 in), and (4.50 in, 1.125 in) that correspond to Reynolds numbers of 43,129, 121,986 and 121,986, and Weber numbers of 4.439×10^6, 17.76×10^6, and 17.76×10^6, respectively.

In most applications of free surface flow such as the dam-breaking problem under study, the free surface might sweep through a great part of the computational domain at all possible inclinations. Under such a situa-

tion, fine grid meshes are needed not only in the wall region but also in the entire flow field. Thus, the use of a square uniform Cartesian grid system

$$\Delta x_i = \Delta x = \Delta y_j = \Delta y \tag{23}$$

is suggested for simplicity of computation. In the present study, the partial-slip condition (7a) and (7b) is employed in the region $x_{i-2} \leqslant x \leqslant x_{i+3}$ provided that the liquid front is in the interval $x_i < x_f < x_{i+1}$. The receding water front on the vertical wall is defined similarly. The uniform time step $\Delta\tau = 0.025$ is found adequate for all the three cases.

In the case of $(H, W) = (2.25\text{ in}, 2.25\text{ in})$, three grid meshes, namely, 61×31, 81×41 and 101×51 grid points, are employed on the domain of $0 \leqslant x \leqslant 4$ and $0 \leqslant y \leqslant 2$. This implies the grid sizes of $\Delta x = \Delta y = 0.0667, 0.05$ and 0.04, respectively. The resulting solutions of pressure and velocity based on $\Delta x = \Delta y = 0.05$

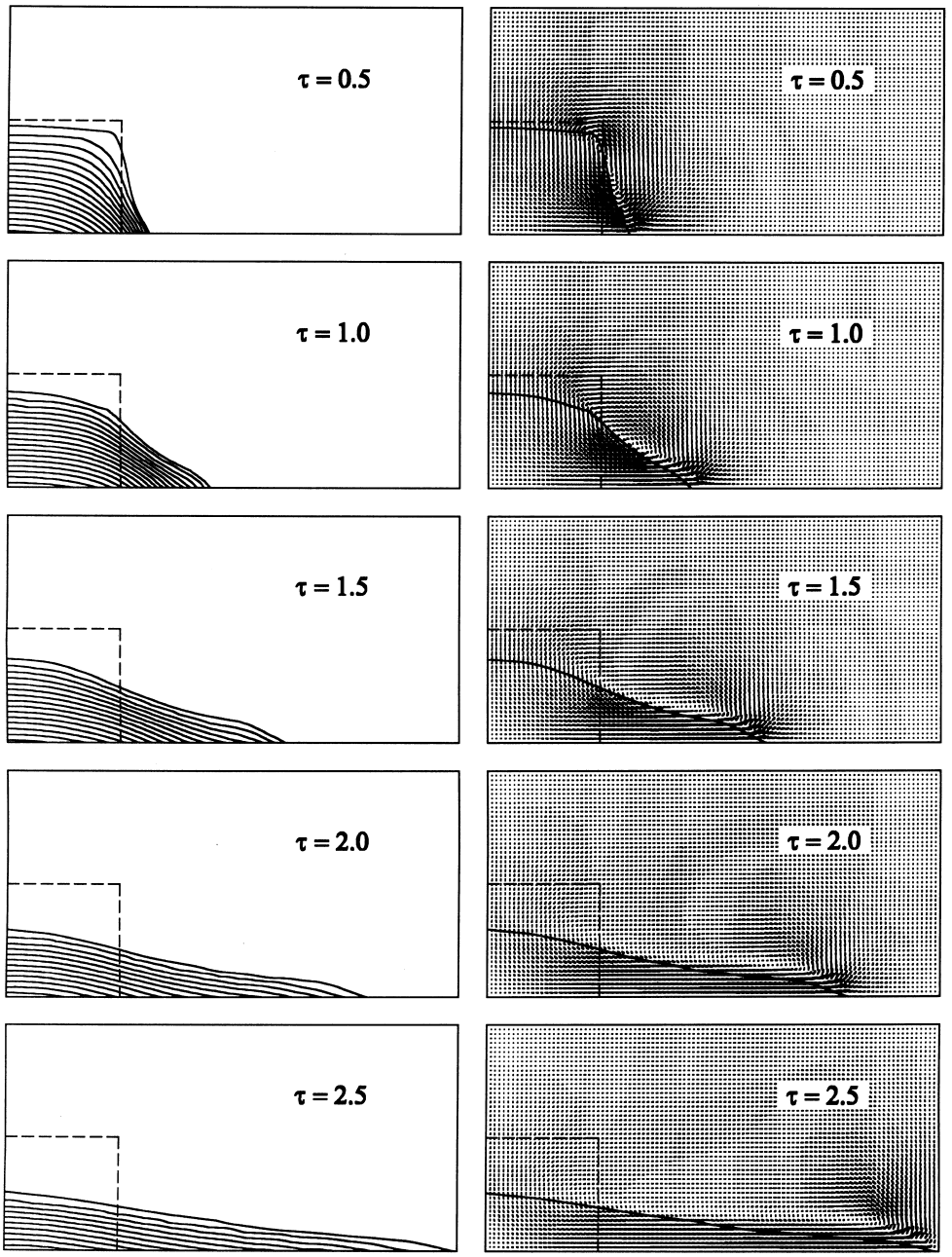

Fig. 3. (a) Isobars with increment of $\Delta p = 0.05$. (b) Velocity vectors at various times for the case $(H, W) = (2.25\text{ in}, 2.25\text{ in})$.

are presented, respectively, in Fig. 3(a) and (b) for $\tau = 0.5, 1.0, 1.5, 2.0$ and 2.5. The increment of the isobars employed in Fig. 3(a) is $\Delta p = 0.05$. Influence of grid mesh will be discussed later. As observable from Fig. 3(a), the pressure is essentially zero in the air region. This can be attributed to the negligible density and viscosity of the air as compared to the water. It is interesting to note from Fig. 3(b) that the continuity equation (2) induces a vortex in a layer of air adjacent to the free surface. This finding is consistent with the physical reasoning.

In their experiment, Martin and Moyce [12] constrained the water column with a thin waxed paper diaphragm. A 36 V bank of car batteries was shorted momentarily to free the waxed paper and thus allowed the flow to begin. The times were recorded when the liquid front reached some fixed locations after the current was applied. Unfortunately, in view of the very heavy currents drawn from the batteries and the nature of the diaphragm construction Martin and Moyce [12] found it was impossible to record the exact "beginning time" of the flow motion after the current application. Furthermore, such a time lag varied from one run to another in the experiment. To circumvent this difficulty, Martin and Moyce [12] normalized their experimental data by setting $x_f(0.8) = 1.44$ for all the 12 runs performed for the case $(H, W) = (2.25 \text{ in}, 2.25 \text{ in})$, i.e. setting $\tau = 0.80$ when the liquid front reached the particular location $x = 1.44$. The normalized data of the 12 runs as well as their mean value can be found in [12, Table 1]. Three photographs after current application also were provided in [12] with unknown times when the shots were taken.

Fig. 4 shows the resulting water front $x_f(\tau)$ of the present study on various grid meshes $(\Delta x = \Delta y = 0.04, 0.05, 0.067)$ for the case of a square water column $H = W = 2.25$ in. The available experimental data [12] and the existing numerical results such as the standard MAC method [5], the net inflow method [11], the CSF method [13] and the modified MAC method [6] are plotted also in Fig. 4. As mentioned in the previous paragraph, the experimental data of Martin and Moyce [12] has been normalized with $x_f(0.8) = 1.44$. Thus, comparison with the experimental data on the front speed (slope of the $x_f(\tau)$ curve) would be more practical than that on the water front itself $x_f(\tau)$.

From Fig. 4, it is found that the grid mesh of $\Delta x = \Delta y = 0.05$ is adequate for the present case. Fig. 4 reveals also that the front speed of the present prediction is slightly faster than the measurement [12] at the beginning of the flow. Nevertheless, a good agreement between them can be observed for $\tau > 1.2$. The MAC method [5,6] seems to overpredict the advancement of the water front for the present case. By contrast, the result based on the net inflow method [11] agrees with the present study very well. However, the net inflow method is seen to produce an oscillating curve for the water front $x_f(\tau)$. The CSF method [13] gives rise to a faster front speed up to $\tau = 0.4$ and thereafter a slower front speed as compared to the present result.

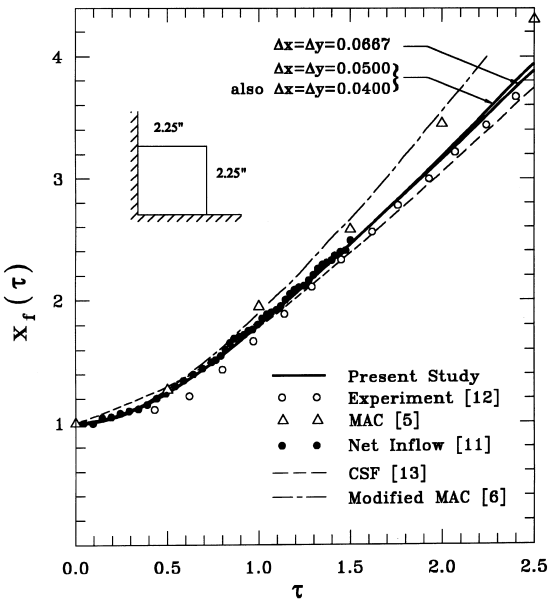

Fig. 4. Comparison of the water front $x_f(\tau)$ among the present result and experimental data and existing numerical results for the case $(H, W) = (2.25 \text{ in}, 2.25 \text{ in})$.

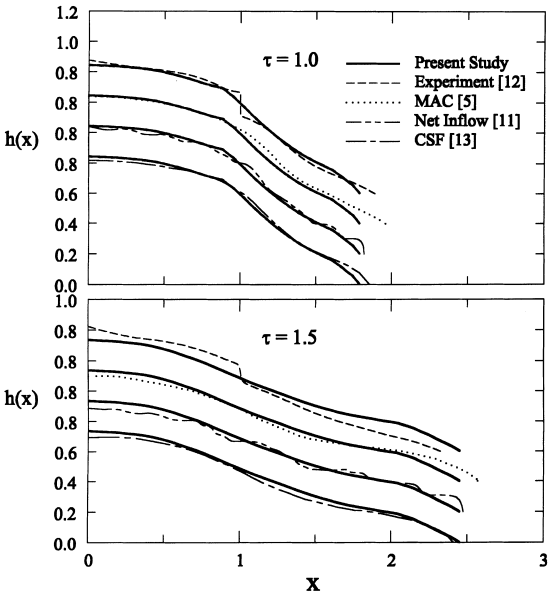

Fig. 5. Comparison of free surface profiles $h(x)$ at $\tau = 1.0$ and $\tau = 1.5$ between the present result and the experimental data and each of the existing numerical results for the case $(H, W) = (2.25 \text{ in}, 2.25 \text{ in})$.

Fig. 5 shows a comparison on the free surface profile $h(x)$ at the two times $\tau = 1.0$ and $\tau = 1.5$ between the present result and each of the existing numerical solutions based on the MAC method [5], the net inflow method [11] and the CSF method [13]. Experimental data traced from two of the photographs provided by Martin and Moyce [12] are plotted in Fig. 5 also as a reference. The actual shooting times when the two shots were taken, however, are not known. Nevertheless, they are estimated to be $\tau = 1.14$ and $\tau = 1.45$ from the normalized water front measurement $x_f(\tau)$.

It should be noted here that a jump in the free surface profile at $x = 1$ is clearly observed from the photograph [12]. It seems to arise from the remains of the broken diaphragm after current application. This might account for the delay of the water front x_f at the beginning of the dam-breaking flow as shown in Fig. 4. Satisfactory agreements between the present result and the existing numerical solutions [5,11,13] on the free surface profile are observable. However, the net inflow method [11] poses a vertical water front that seems to be physically unrealistic.

In the second case of $(H, W) = (4.5 \text{ in}, 2.25 \text{ in})$, 101×41 points are employed on the computational domain of $0 \leqslant x \leqslant 10/3$ and $0 \leqslant y \leqslant 4/3$. The corresponding grid size is $\Delta x = \Delta y = 1/30$. The resulting isobars (with the increment $\Delta p = 0.05$) and the velocity based on the present numerical procedure are depicted in Fig. 6. Their counterparts in the third case $(H, W) = (4.5 \text{ in}, 1.125 \text{ in})$ with the same increment $\Delta p = 0.05$ are provided in Fig. 7. Note that the numerical procedure for the third case is performed on the computational domain of $0 \leqslant x \leqslant 2.5$ and $0 \leqslant y \leqslant 1.25$ with a Cartesian grid system of 101×51 grid points ($\Delta x = \Delta y = 0.025$). The characteristics of the numerical results of the latter two cases are found to be similar to that of the first one.

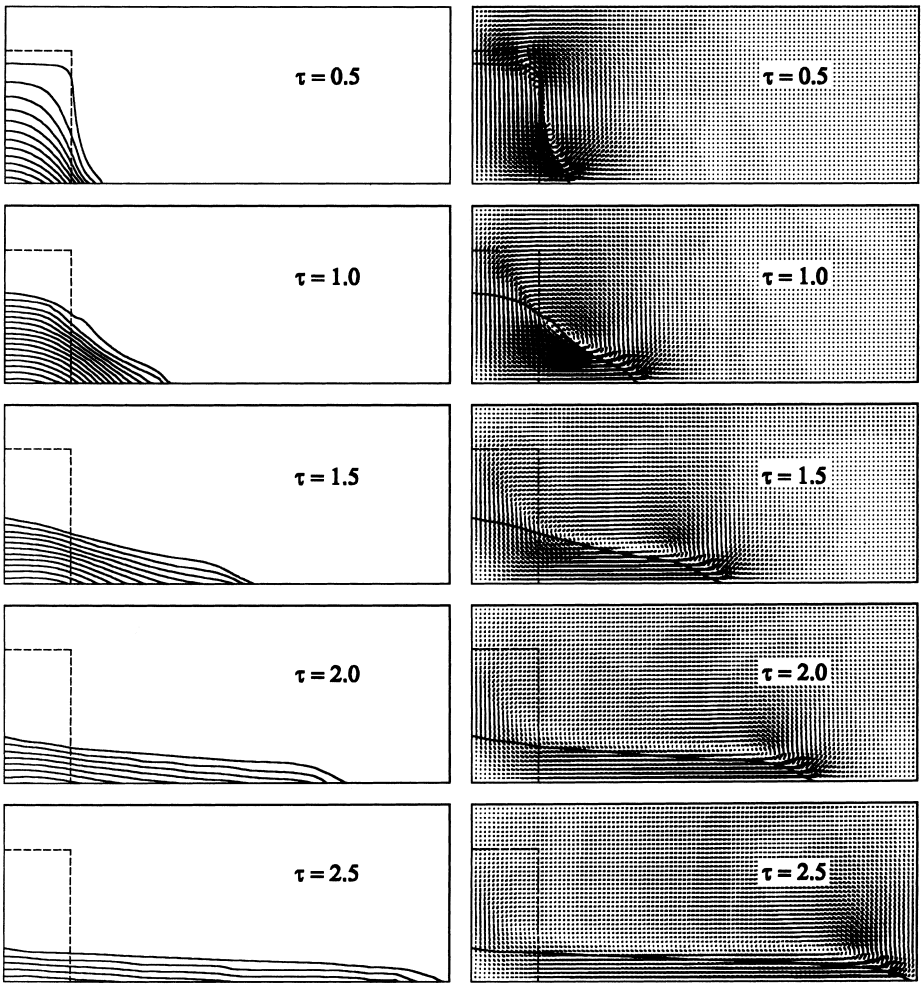

Fig. 6. Isobars with increment of $\Delta p = 0.05$ and velocity vectors at various times for the case $(H, W) = (4.5 \text{ in}, 2.25 \text{ in})$.

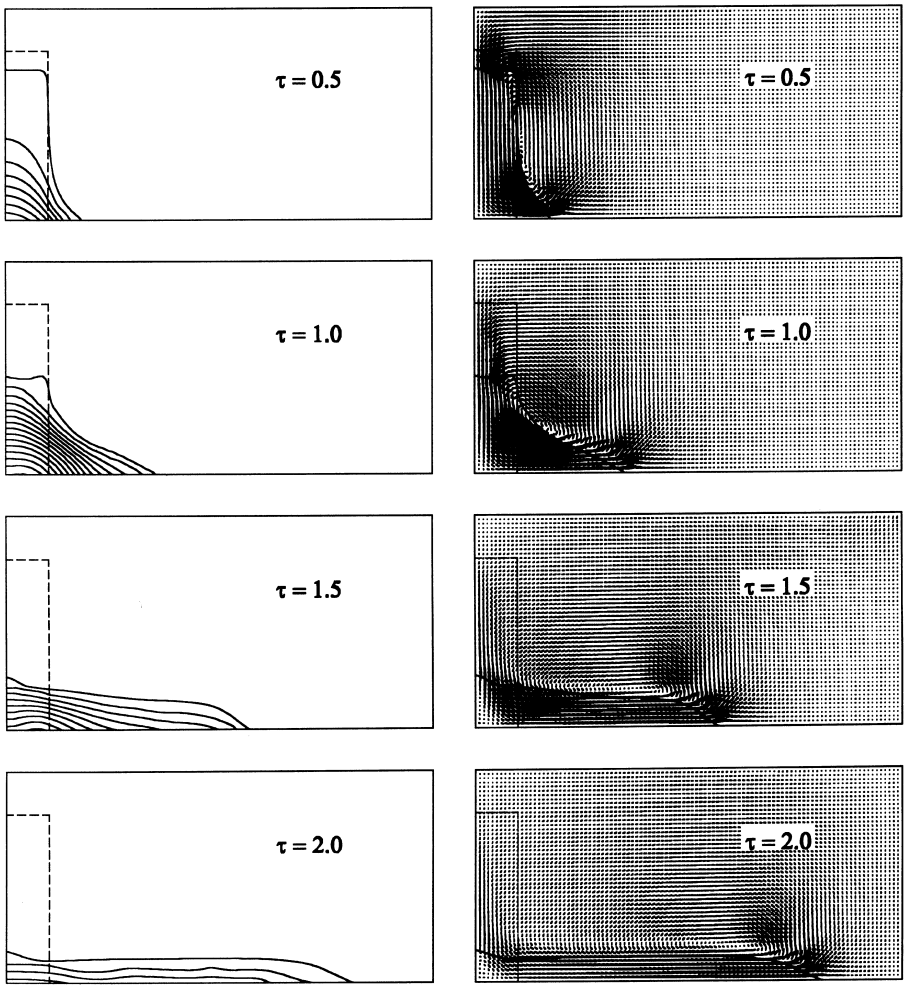

Fig. 7. Isobars with increment of $\Delta p = 0.05$ and velocity vectors at various times for the case $(H, W) = (4.5 \text{ in}, 1.125 \text{ in})$.

Finally, comparisons of water front results among the present prediction and the available experiment [12] and the numerical predictions by the VOF method [9] and the modified MAC method [6] are shown in Fig. 8 for the second case $(H, W) = (4.5 \text{ in}, 2.25 \text{ in})$. For convenience, a comparison between the predicted water front from the present study and that from the measurement [12] for the third case $(H, W) = (4.5 \text{ in}, 1.125 \text{ in})$ is presented also in Fig. 8. Note that the experimental data have been normalized with $x_f(0.595) = 0.72$ for the second case and $x_f(0.5) = 0.36$ for the third one, while both cases have the same Reynolds number $Re = 121,986$. Again, satisfactory agreements on the front speed are found to exist between the experimental data [12] and the present prediction for both cases. The VOF method by Hirt and Nichols [9] seems to overpredict the water front, while the modified MAC method [6] predicts a slower water front as compared to the present prediction.

6. Conclusion

A single set of governing equations covering both liquid and air is derived for viscous incompressible free surface flow without smearing the free surface. The momentum equations are solved with an extended weighting function scheme on a fixed and nonstaggered Cartesian grid system. The NAPPLE algorithm is then applied for the pressure solution. Through the use of the NAPPLE algorithm, effect of the surface tension is imposed on the free surface. Such a numerical technique has shown good performance in handling the discontinuities of the physical properties across the free surface. To achieve an accurate free surface profile for the next time step, a harmonic function is proposed to extrapolate the migration velocity for the free surface from the grid points adjacent to the free surface on the liquid side. From the three cases of dam-breaking problem, the present numerical method is seen to predict a water

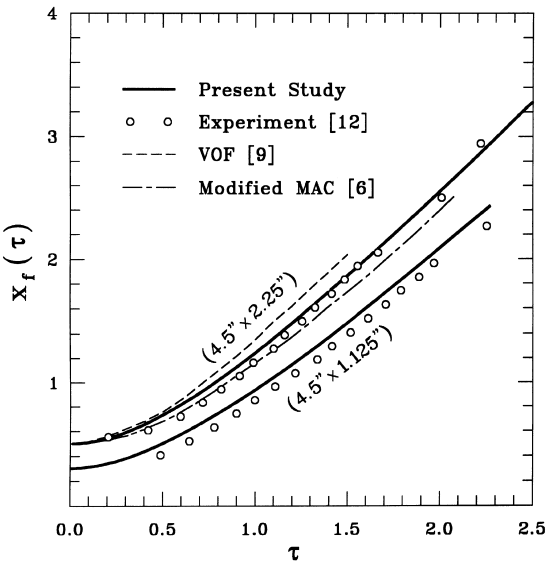

Fig. 8. Comparison of the water front $x_f(\tau)$ among the present result and experimental data and existing numerical results for the cases of $(H, W) = (4.5 \text{ in}, 2.25 \text{ in})$ and $(4.5 \text{ in}, 1.125 \text{ in})$.

front that satisfactorily agrees with the well-known experimental data. Furthermore, an induced vortex in a layer of air adjacent to the free surface is obtained. In the present formulation, the "free surface" is treated as an internal boundary, and thus no additional treatment is needed for the shear stresses on the free surface. Formulation of the present numerical method is quite simple. It can be easily extended to three-dimensional viscous free surface flow, even inside a cavity of arbitrary shape.

Acknowledgements

The authors wish to express their appreciation to Professor M. J. Andrews and Professor H. C. Chen of Texas A&M University for their valuable comments and discussions. This work was supported by the National Science Council of Taiwan through the project NSC 89-2212-E007-032.

References

[1] M.J. Fritts, J.P. Boris, The Lagrangian solution of transient problems in hydrodynamics using a triangular mesh, J. Comput. Phys. 31 (1979) 173–215.

[2] D.E. Fyfe, E.S. Oran, M.J. Fritts, Surface tension and viscosity with Lagrangian hydrodynamics on a triangular mesh, J. Comput. Phys. 76 (1988) 349–384.

[3] R.W. Lewis, S.E. Navti, C. Taylor, A mixed Lagrangian–Eulerian approach to modelling fluid flow during mould filling, Int. J. Numer. Meth. Fluids 25 (1997) 931–952.

[4] C.W. Chen, C.R. Li, T.H. Han, C.T. Shei, W.S. Hwang, C.M. Houng, Numerical simulation of filling pattern for an industrial die casting and its comparison with the defects distribution of an actual casting, Trans. Am. Foundrymen's Soc. 104 (1994) 139–146.

[5] F.H. Harlow, J.E. Welch, Numerical calculation of time-dependent viscous incompressible flow of fluid with free surface, Phys. Fluids 8 (1965) 2182–2189.

[6] T. Nakayama, M. Mori, An Eulerian finite element method for time-dependent free surface problems in hydrodynamics, Int. J. Numer. Meth. Fluids 22 (1996) 175–194.

[7] F.H. Harlow, A.A. Amsden, J.R. Nix, Relativistic fluid dynamics calculations with the particle-in-cell technique, J. Comput. Phys. 20 (1976) 119–129.

[8] P.E. Raad, S. Chen, D.B. Johnson, The introduction of micro cells to treat pressure in free surface fluid flow problems, ASME J. Fluids Eng. 117 (1995) 683–690.

[9] C.W. Hirt, B.D. Nichols, Volume of fluid (VOF) method for the dynamics of free boundaries, J. Comput. Phys. 39 (1981) 201–225.

[10] E. Broyer, C. Gutfinger, Z. Tadmore, A theoretical model for the cavity filling process in injection molding, Trans. Soc. Rehol. 19 (1975) 423–444.

[11] S.P. Wang, K.K. Wang, A net inflow method for incompressible viscous flow with moving free surface, Int. J. Numer. Meth. Fluids 18 (1994) 669–694.

[12] J.C. Martin, W.J. Moyce, An experimental study of the collapse of liquid columns on a rigid horizontal plane, Philos. Trans. Roy. Soc. London 244A (1952) 312–324.

[13] J. Wu, S.T. Yu, B.N. Jiang, Simulation of two-fluid flows by the least-square finite element methods using a continuum surface tension model, NASA CR-202314 Lewis Research Center. Cleveland, Ohio, 1996.

[14] J.U. Brackbill, D.B. Kothe, C. Zemach, A continuum method for modeling surface tension, J. Comput. Phys. 100 (1992) 335–354.

[15] D. Jacqmin, Three-dimensional computations of droplet collisions, coalescence, and droplet/wall interactions using a continuum surface-tension method, AIAA paper No. 95-0883, 1995.

[16] S.O. Unverdi, G. Tryggvason, A front-tracking method for viscous, incompressible, multi-fluid flows, J. Comput. Phys. 100 (1992) 25–37.

[17] M. Sussman, E. Fatemi, P. Smereka, S. Osher, An improved level set method for incompressible two-phase flows, Comput. Fluids 27 (1998) 663–680.

[18] H. Haj-hariri, Q. Shi, A. Borhan, Effect of local property smearing on global variables: implication for numerical simulations of multiphase flows, Phys. Fluids 6 (1994) 2555–2557.

[19] S.L. Lee, R.Y. Tzong, An enthalpy formulation for phase change problems with a large thermal diffusivity jump across the interface, Int. J. Heat Mass Transfer 34 (1991) 1491–1502.

[20] S.L. Lee, Weighting function scheme and its application on multidimensional conservation equations, Int. J. Heat Mass Transfer 32 (1989) 2065–2073.

[21] S.L. Lee, R.Y. Tzong, Artificial pressure for pressure-linked equation, Int. J. Heat Mass Transfer 35 (1992) 2705–2716.
[22] S.L. Lee, A strongly-implicit solver for two-dimensional elliptic differential equations, Numer. Heat Transfer 16B (1989) 161–178.
[23] T. Sarpkaya, Vorticity, free surface and surfactants, Ann. Rev. Fluid Mech. 28 (1996) 83–128.
[24] W.T. Tsai, D.K.P. Yue, Computation of nonlinear free-surface flows, Ann. Rev. Fluid Mech. 28 (1996) 249–278.
[25] A. Castrejon, M.J. Andrews, A procedure for calculating moving-interface flows with PHOENICS-84, in: Markatos, Tatchell, Cross and Rhodes (Eds.), Numerical Simulation of Fluid and Heat/Mass Transfer Processes. Lecture Notes in Engineering, vol. 18. Springer, Berlin, 1986, pp. 433–443.